

AlM₂B₂ (M=Cr, Mn, Fe, Co, Ni): a group of nanolaminated materials

Krisztina Kádas^{a,*}, Diana Iuşan^a, Johan Hellsvik^b, Johan Cedervall^c, Pedro Berastegui^c, Martin Sahlberg^c, Ulf Jansson^c, Olle Eriksson^a

^a*Division of Materials Theory, Department of Physics and Astronomy, Uppsala University, Box 516, SE-751 20, Uppsala, Sweden*

^b*Department of Materials and Nanophysics, School of Information and Communication Technology, Electrum 229, Royal Institute of Technology (KTH), SE-164 40 Kista, Sweden*

^c*Department of Chemistry - The Ångström Laboratory, Uppsala University, Box 538, 751 21 Uppsala, Sweden*

Abstract

Combining theory with experiments, we study the phase stability, elastic properties, electronic structure and hardness of layered ternary borides AlCr₂B₂, AlMn₂B₂, AlFe₂B₂, AlCo₂B₂, and AlNi₂B₂. We find that the first three borides of this series are stable phases, while AlCo₂B₂ and AlNi₂B₂ are metastable. We show that the elasticity increases in the boride series, and predict that AlCr₂B₂, AlMn₂B₂, and AlFe₂B₂ are more brittle, while AlCo₂B₂ and AlNi₂B₂ are more ductile. We propose that the elasticity of AlFe₂B₂ can be improved by alloying it with cobalt or nickel, or a combination of them. We present evidence that these ternary borides represent nanolaminated systems. Based on SEM measurements, we demonstrate that they exhibit the delamination phenomena, which leads to a reduced hardness compared to transition metal mono- and diborides. We discuss the background of delamination by analyzing chemical bonding and theoretical work of separation in these borides.

Keywords: Nanolaminated ternary borides, Phase stability, Elastic constants, Hardness, Scanning electron microscopy

1. Introduction

Compounds with a layered structure have a potential to act as nanolaminated materials with unique properties. The most well known nanolaminates are the so-called MAX

*Corresponding author

Email address: Krisztina.Kadas@physics.uu.se (Krisztina Kádas)

phases [1]. They are ternary metal carbides or nitrides of the general formula $M_{n+1}AX_n$ with $n=1, 2$ or 3 , where M is a transition metal, A is a group A element, and X is either carbon or nitrogen. MAX phases have unique chemical and physical properties such as high electrical and thermal conductivity, high thermal shock resistance and damage tolerance, machinability, high oxidation resistance, etc. Many MAX phases also exhibit special deformation properties characterized by basal slip, kink and shear band deformation, and delaminations of individual grains [1]. These properties can be explained by the nanolaminated structure where MX slabs with strong M-X bonds are separated by A-layers with weaker M-A bonds.

Another group of compounds, which potentially can exhibit a similar type of properties are metal borides. In fact, Telle and co-workers showed that W_2B_5 with alternating W and boron layers, has similar mechanical properties as MAX phases [2], and that this phase also exhibits delamination phenomena. Furthermore, Ade and Hillebrecht recently proposed that ternary borides, such as Cr_2AlB_2 , Cr_3AlB_4 , and Cr_4AlB_6 , exhibit nanolaminated structures. They called these ternary borides MAB phases in analogy to the more well-known MAX phases [3]. Very recently, $MoAlB$ was shown to represent a nanolaminated system [4, 5], and Lu and co-workers also measured the atomic structure of nanolaminated $AlCr_2B_2$ and $AlFe_2B_2$ [5].

The ternary AlM_2B_2 borides include in fact several known phases with $M=Cr, Mn$ and Fe . The crystal structure of $AlFe_2B_2$ is shown in Fig. 1, where the analogy to the MAX phases is clearly seen with Fe-B slabs separated by Al layers. There are strong B-B and Fe-B bonds in the boride slabs, which are separated with much weaker Fe-Al and Al-B bonds. The interest in this group of ternary borides has increased after $AlFe_2B_2$ was presented as a possible magnetocaloric material exhibiting a large magnetocaloric effect [6, 7]. Tan et al. found that $AlFe_2B_2$ is a soft ferromagnet with the ordering temperature of 282 K and 307 K, and a saturation magnetization of $1.515 \mu_B$ or $1.03 \mu_B$ per Fe atom, depending on the synthesis method. They also investigated other ternary borides, and reported the calculated magnetic properties and electronic structures of $AlMn_2B_2$, $AlCr_2B_2$ and $AlFe_{2-x}Mn_xB_2$ [8]. The authors of Ref. [8] found that $AlMn_2B_2$ and $AlCr_2B_2$ are nonmagnetic, and in $AlFe_{2-x}Mn_xB_2$ both the saturation magnetization and the ferromagnetic ordering temperature gradually decreases with increasing Mn content. However,

they did not study the phase stability of the ternary borides. The mechanical properties of ternary AlM_2B_2 borides are also not systematically described previously. Nie et al. calculated the elastic properties of AlCr_2B_2 [9], while Cheng et al. published theoretical elastic constants for AlFe_2B_2 [10]. The elastic properties of the other ternary AlM_2B_2 borides, however, are not known.

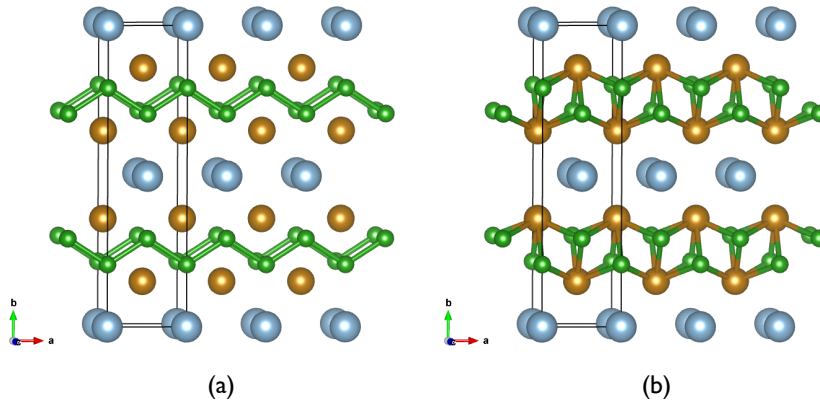


Figure 1: (Color online.) Crystal structure of AlFe_2B_2 . The unit cell is shown by black lines. Al, Fe and B atoms are displayed by blue, brown, and green, respectively. The boron-boron bonds are shown on panel (a), while the Fe-B bonds are displayed on panel (b).

The aim of this study is to present a systematic study of the AlM_2B_2 (M=Cr, Mn, Fe, Co, and Ni) phases using density functional theory (DFT) based methods combined with experimental studies. We calculate the unit cell parameters of the borides, and compare them with those measured for experimentally synthesized samples. We calculate the phase stability, elastic properties and electronic structure of these ternary borides, and analyze their chemical bonding. We also measure the hardness of the experimental samples, and characterize them by means of scanning electron microscopy (SEM). Finally, we discuss the nanolaminated structure and behavior of these borides and their similarities to MAX-phases.

2. Computational details

We performed first principle calculations by means of the projector augmented wave [11, 12] method as implemented in the Vienna ab initio simulation package [13, 14, 15]. This method is based on the density functional theory [16, 17]. To calculate the exchange-correlation energy, the generalized gradient approximation with the Perdew, Burke, and Ernzerhof functional [18] was used. We employed a plane-wave energy cutoff of 500 eV and used a Monkhorst-Pack grid of 16x8x16 to sample the Brillouin zones for geometry optimizations, and a larger grid 30x30x30 for elastic constant and electronic structure calculations. The conjugate-gradient method was applied to relax the atoms into their optimal positions until the forces on all atoms were smaller than 0.005 eV/Å. We calculated the nine independent elastic constants c_{11} , c_{22} , c_{33} , c_{44} , c_{55} , c_{66} , c_{12} , c_{13} and c_{23} as described in Ref. [19]. Accordingly, we employed small strains to the equilibrium lattice, and deduced the elastic constants from the calculated total energies of the distorted lattices. In addition, magnetic moments were also calculated using the full-potential linear muffin-tin orbital (FP-LMTO) code RSPt [20, 21].

In order to investigate the chemical bonding between the atomic constituents, we have carried out crystal orbital Hamilton population (COHP) calculations using the LOBSTER code [22, 23, 24, 25]. To determine work of separation (W) in AlM_2B_2 borides, we calculated the energy cost of separating these crystals by 20 Å vacuum between different layers perpendicular to crystallographic axis b . Upon separation, atoms of the first two layers at the interfaces were allowed to relax, while the rest of the atoms were kept fixed.

3. Experimental

Samples were synthesized by arc-melting stoichiometric amounts of chromium (Alfa Aesar, purity 99.995%), manganese (Institute of Physics, Polish Academy of Sciences, purity 99.999%), iron (Leico Industries, purity 99.995%. Surface oxides were reduced in H_2 -gas.), cobalt (Johnson Matthey, purity 99,999%) or nickel (ESPI Metals, purity 99,995%), with boron (Wacher-Chemie, purity 99.995%) to their respective metal-boride. The metal borides were then reacted with aluminum (Gränges SM, purity 99.999%) with an excess of 50% aluminum [26] to suppress the formation of secondary phases. All samples were then crushed, pressed into pellets and heat treated in evacuated silica tubes

at 900°C for 14 days. The chromium, manganese and iron samples were then etched in diluted HCl (1:1) to remove impurity phases.

The crystalline phases were analysed with X-ray powder diffraction (XRD) on a Bruker D8 Advance using $\text{CuK}\alpha$ radiation. To precisely determine the unit cell parameters refinements were performed in the program UnitCell [27], this was done after the etching step for the chromium, manganese and iron samples and directly after arc-melting for the cobalt and nickel samples.

The heat treated pieces were remelted, annealed and placed in bakelite and polished for Vickers micro-hardness measurements, which were performed on a Matsuzawa MTX50 with a load of 200 g dwelling for 15 s. The measurements were done 10 times in the same region on each sample and the mean value of the hardness values is reported here. Delamination of the samples were studied with scanning electron microscopy (SEM) using a Zeiss LEO 1550 equipped with an Aztec energy dispersive X-ray spectrometer (EDS). The polished samples were damaged by pressing a sharp diamond tip into the polished sample surface.

4. Results

4.1. Crystal structure

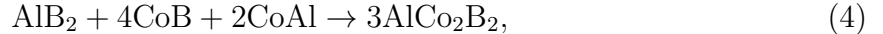
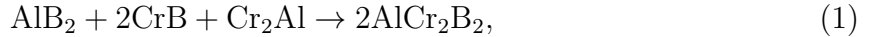
Ternary AlM_2B_2 borides (M=Cr, Mn, Fe) crystallize in an orthorhombic lattice, space group $Cmmm$. The crystal structure of AlFe_2B_2 was first described by Jeitschko in 1969 [28]. These borides have a layered structure, where M-B layers are separated by Al layers. The M-B layers consist of two boron layers between two transition metal layers. In Fig. 1 we show the crystal structure of AlFe_2B_2 . The Fe-B layers include zigzag chains of boron atoms along the crystallographic axis a , which is displayed in Fig. 1a. The B-B bond length in these chains is 1.74 Å. In addition, Fe-B bonds are also formed in the Fe-B layers, as shown in Fig. 1b. Each Fe atom forms six Fe-B bonds with a bond length of 2.16 Å and 2.17 Å, where the shorter bonds are between Fe atoms and B atoms of the boron layer closer to the Fe layer, while the longer Fe-B bonds are formed between Fe atoms and B atoms of the adjacent boron layer. Each B atom is coordinated by six Fe atoms in the Fe-B layers. In the Al layers between the Fe-B layers, each Al atom forms Fe-Al bonds with Fe atoms of both neighboring Fe-B layers, with a bond length of 2.61

Å. Al atoms also form bonds with two axial B atoms of the neighboring Fe-B layers, the Al-B bond lengths being 2.29 Å.

The theoretical and experimental unit cell parameters are listed in Table 1. Theory reproduces the experimental cell parameters well, the maximal deviation being 0.5% in a , 0.1% in b , and 2.4% in lattice parameter c . We note that our measured lattice parameters are very close to those measured by Ade and Hillebrecht [3] the difference being $\leq 0.3\%$, and also to those measured by Chai et al. [8], where the maximal deviation is 0.8%. For the first three borides, namely for AlCr_2B_2 , AlMn_2B_2 , and AlFe_2B_2 , where measured lattice parameters are available, the experimental volume of the unit cell decreases in the series from AlCr_2B_2 to AlFe_2B_2 according to both our experimental results and those published by Ade and Hillebrecht [3], and Chai et al. [8]. In the calculations, however, AlMn_2B_2 has the lowest volume of these three borides, which is due to the fact that its theoretical lattice parameter c is smaller than the experimental one by 2.4%.

4.2. Phase stability

To examine the stability of AlM_2B_2 ($M=\text{Cr, Mn, Fe, Co, Ni}$), we calculate the formation energies (ΔE) from competing binary phases:



where AlB_2 [29] is of $P6/mmm$ structure, MnB [30], FeB [31] and CoB [31] are of $Pnma$ structure, CrB [32] and NiB [33] is of $Cmcm$ structure, Cr_2Al [34] is of $I4/mmm$ structure, MnAl_6 [35] is of $Cmcm$ structure, and finally, FeAl [36], CoAl [37] and NiAl [38] are of

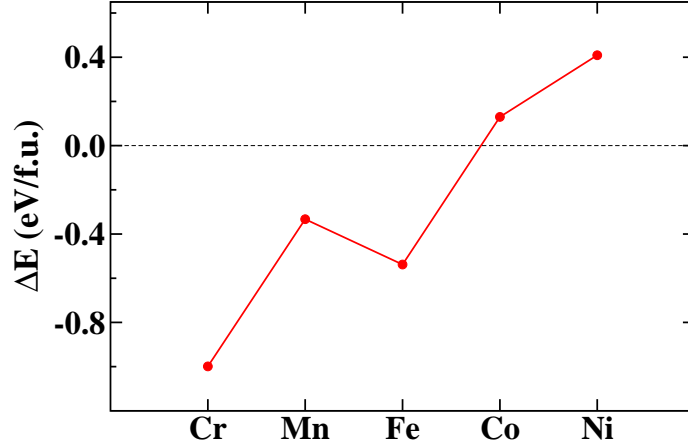


Figure 2: (Color online.) Theoretical formation energies of AlM₂B₂ (M=Cr, Mn, Fe, Co, Ni).

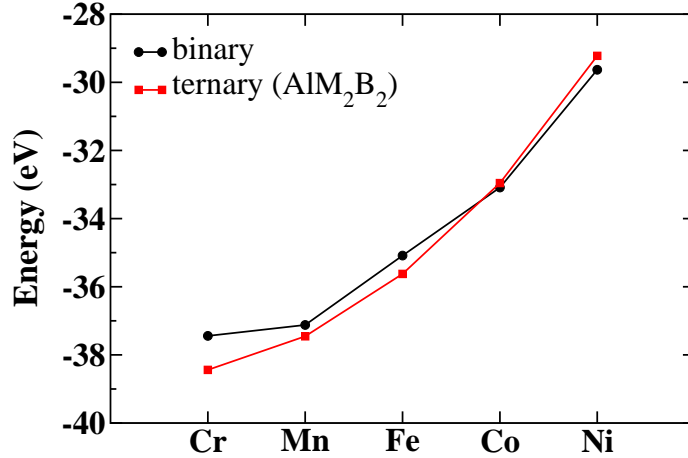


Figure 3: (Color online.) Total energies of the binary phases in reactions 1-5 (black circles) and the ternary AlM₂B₂ phases (red squares).

$Pm\bar{3}m$ (CsCl) structure. A negative formation energy means that AlM₂B₂ represent a stable phase.

We calculate $\Delta E_1=-0.999$ eV/f.u., $\Delta E_2=-0.333$ eV/f.u., $\Delta E_3=-0.538$ eV/f.u. formation energy for reaction 1, 2, and 3, respectively, i.e. AlCr₂B₂, AlMn₂B₂, and AlFe₂B₂ are stable (see Fig. 2). For reactions 4 and 5, however, we obtain positive formation energies (Fig. 2). We calculate $\Delta E_4=0.130$ eV/f.u. for the formation of AlCo₂B₂ (reaction 4), and

$\Delta E_5=0.409$ eV/f.u. for the formation of AlNi_2B_2 (reaction 5). Our results suggest that both AlCo_2B_2 and AlNi_2B_2 are thermodynamically unstable, and at best could be formed as metastable compounds. However, the calculated phase stabilities (Fig. 2) suggest that AlCo_2B_2 and AlNi_2B_2 alloyed with Fe can be stable phases.

In Fig. 3 we plot the calculated total energies of the binary phases in reactions 1-5 corresponding to one formula unit of AlM_2B_2 (left-hand sides in Eqs. 1-5), together with the energies of the ternary AlM_2B_2 phases (right-hand sides in Eqs. 1-5). Figure 3 shows that the energy of the ternary phases increases in the series, i.e. from AlCr_2B_2 to AlNi_2B_2 , and the stability of AlCr_2B_2 , AlMn_2B_2 and AlFe_2B_2 is due to the high energy of the corresponding binary phases.

4.3. Elastic properties

The calculated single crystal elastic constants c_{ij} are shown in Table 2. The elastic constant c_{11} is larger than the other two principal elastic constants c_{22} and c_{33} in all ternary borides. This means that the AlM_2B_2 crystals are harder to compress along axis a , than along axes b or c , which is in line with the fact that the strong boron-boron bonds can be found along axis a in these crystals. We note that Cheng et al. [10] found $c_{22} > c_{11} > c_{33}$ in AlFe_2B_2 , in contrast to our results, which could be due to a smaller number of k-points that they applied to calculate the elastic constants, compared to what we used. We find that the shear elastic constants are significantly smaller than the principal ones in all AlM_2B_2 borides, see Table 2. Our theoretical elastic constants for AlCr_2B_2 agree with those calculated by Nie et al. [9], the deviation being less than 3% in the principal elastic constants, and less than 10% in the shear elastic constants. The difference may again be due to the smaller k-mesh employed in Ref. [9].

For an orthorhombic crystal, the criteria for mechanical stability are $c_{11} > 0$, $c_{11} + c_{22} > c_{22}^2$, $c_{11}c_{22}c_{33} + 2c_{12}c_{13}c_{23} - c_{11}c_{23}^2 - c_{22}c_{13}^2 - c_{33}c_{12}^2 > 0$, $c_{44} > 0$, $c_{55} > 0$, $c_{66} > 0$ [39]. All of these stability criteria are fulfilled in all the ternary borides examined in this paper, which means that AlCr_2B_2 , AlMn_2B_2 , AlFe_2B_2 , AlCo_2B_2 , and AlNi_2B_2 are mechanically stable. Note that this is not equivalent to the phase stability discussed above.

From the single crystal elastic constants and the elastic compliance constants s_{ij} , we also calculated the polycrystalline elastic constants, namely the bulk moduli (B) and shear moduli (G) according to the Voigt (B_V , G_V) [40] and Reuss approximations (B_R ,

G_R) [41], which correspond to the upper and lower limit of the elastic moduli. Hill's bulk (B_H) and shear moduli (G_H) are the average of the Voigt and Reuss bounds, i.e. $B_H = \frac{1}{2}(B_R + B_V)$, and $G_H = \frac{1}{2}(G_R + G_V)$. The Young's modulus (E) and Poisson ratio (ν) for an isotropic material is then

$$E_{V,R,H} = \frac{9B_{V,R,H}G_{V,R,H}}{3B_{V,R,H} + G_{V,R,H}}, \quad (6)$$

and

$$\nu_{V,R,H} = \frac{3B_{V,R,H} - 2G_{V,R,H}}{2(3B_{V,R,H} + G_{V,R,H})}. \quad (7)$$

The calculated polycrystalline elastic constants are listed in Table 3. The bulk modulus to shear modulus ratio, B/G , is an important measure of elasticity of a material, it can be employed to characterize the deformation behavior of a crystal. Materials with a $B/G < 1.75$ are expected to be brittle, while materials with $B/G > 1.75$ are ductile. Analyzing the bulk and shear moduli, we find that both B and G decrease in the series, i.e. from AlCr_2B_2 to AlNi_2B_2 , but the shear modulus decreases to a larger extent (see inset in Fig. 4). While B_H decreases with 16.7%, comparing AlNi_2B_2 to AlCr_2B_2 , we obtain a 53.2% decrease for the shear modulus G_H . Accordingly, B/G increases in the series, except for AlNi_2B_2 , which has a slightly smaller B/G than AlCo_2B_2 (see Fig. 4 and Table 3). The relatively high B/G calculated for AlCo_2B_2 is due to its low shear modulus and high bulk modulus. Based on the theoretical B/G ratios, we expect that AlCr_2B_2 , AlMn_2B_2 , and AlFe_2B_2 are more brittle, while AlCo_2B_2 and AlNi_2B_2 are more ductile. The relatively low B/G calculated for AlFe_2B_2 is due to its low bulk modulus (see inset in Fig. 4). Based on our results, the elasticity of AlFe_2B_2 , which is the last stable boride of the series, can be improved, in fact it should be possible to be made ductile by alloying it with Co, or Ni, or a combination of them.

The Young's modulus, E , characterizes the bond strength of materials. We obtain a decreasing trend in the theoretical Young's moduli from AlCr_2B_2 to AlNi_2B_2 . We will discuss bond strengths in detail in the following section.

In general, the Poisson ratio is a measure of the stability of a crystal against shear. Our calculated Poisson ratio follows an increasing trend from AlCr_2B_2 to AlCo_2B_2 , and AlNi_2B_2 has a slightly lower ν than AlCo_2B_2 (Table 3). Accordingly, the stability against shear decreases in the series.

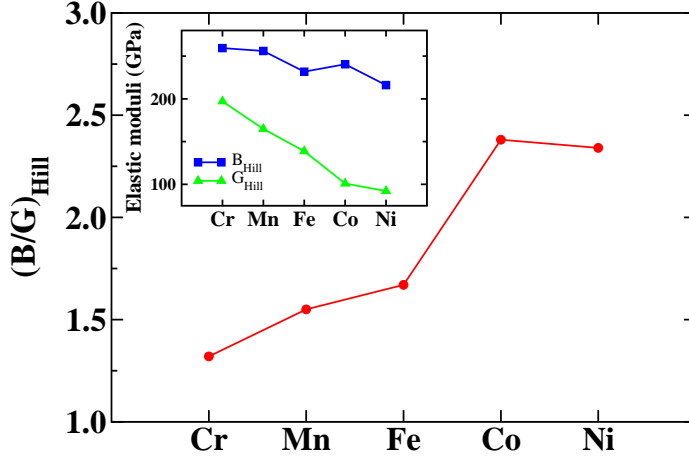


Figure 4: (Color online.) Theoretical B/G (Hill averages) of AlM_2B_2 . Inset: calculated bulk moduli (B) and shear moduli (G) of AlM_2B_2 .

The shift from brittle to ductile behavior from AlCr_2B_2 to AlNi_2B_2 finds further support from the analysis of Cauchy pressures. In orthorhombic materials, the Cauchy pressure can be defined for the three different directions: $P_a=c_{23}-c_{44}$, $P_b=c_{13}-c_{55}$, and $P_c=c_{12}-c_{66}$. In general, a positive Cauchy pressure is an indication of ductile behavior. In AlCr_2B_2 , the Cauchy pressure is negative for all the three directions, showing that this material is more brittle. In AlMn_2B_2 , P_c one of the Cauchy pressures, namely P_c , is positive. In the next boride of the series, AlFe_2B_2 , we obtain positive Cauchy pressure in two directions, here $P_a > 0$ and $P_c > 0$. In the last two borides, AlCo_2B_2 and AlNi_2B_2 , the Cauchy pressure is positive in all the three directions. This is in line with the increasing trend of the B/G ratio we showed above.

It is established that elastic anisotropy plays an important role in the formation of microcracks in ceramics [42]. Hence, to contribute to the understanding of the mechanical properties of AlM_2B_2 ternary borides, in the following we will analyze their anisotropy. The shear anisotropic factors measure the degree of anisotropy in the bonding between atoms in different planes. The shear anisotropic factor for the $\{100\}$ shear planes between the $\langle 011 \rangle$ and $\langle 010 \rangle$ directions is [19]

$$A_1 = \frac{4c_{44}}{c_{11} + c_{33} - 2c_{13}}, \quad (8)$$

for the $\{010\}$ shear planes between the $\langle 101 \rangle$ and $\langle 001 \rangle$ directions it is

$$A_2 = \frac{4c_{55}}{c_{22} + c_{33} - 2c_{23}}, \quad (9)$$

and finally for the $\{001\}$ shear planes between the $\langle 110 \rangle$ and $\langle 010 \rangle$ directions it is

$$A_3 = \frac{4c_{66}}{c_{11} + c_{22} - 2c_{12}}. \quad (10)$$

For an isotropic crystal $A_i=1$, where $i=1-3$. For anisotropic crystals A_i can be larger or smaller than one, the difference being a measure of the degree of elastic anisotropy of the crystal. Our calculated shear anisotropic factors are shown in Table 5. We find that all AlM_2B_2 ternary borides are elastically anisotropic. In most borides we obtain the highest values for the $\{010\}$ shear planes (A_2), except in AlMn_2B_2 , where A_3 is the highest.

In Table 5 we also list the percentage anisotropy in compressibility ($A_B=(B_V-B_R)/(B_V+B_R)$), and in shear ($A_G=(G_V-G_R)/(G_V+G_R)$), introduced by Chung and Buessem [43]. A_B and A_G varies between 0 and 100%, zero representing an isotropic crystal. The highest anisotropy in compressibility is around one percent, we calculate $A_B=1.09\%$ in AlNi_2B_2 , and $A_B=0.93\%$ in AlFe_2B_2 . We obtain higher anisotropies in shear, and we find that A_G increases in the boride series, from AlCr_2B_2 to AlNi_2B_2 . Furthermore, AlCo_2B_2 and AlNi_2B_2 have significantly higher anisotropies than the first three borides, we calculate $A_G=4.72\%$ in AlCo_2B_2 , and $A_G=4.82\%$ in AlNi_2B_2 . Finally, we also calculated the universal anisotropy index, $A_u = 5\frac{G_V}{G_R} + \frac{B_V}{B_R} - 6$, introduced by Ranganathan and Ostoja-Starzewski [44]. A_u can be positive or zero, zero representing an isotropic crystal, and accounts for both compressibility and shear contributions. A_u changes similarly to A_G in the boride series, i.e. it increases from AlCr_2B_2 to AlNi_2B_2 , with AlCo_2B_2 and AlNi_2B_2 having notably higher anisotropies (0.50 and 0.53, respectively) than the other three borides.

To estimate the hardness of AlM_2B_2 ternary borides, we can apply different macroscopic models for hardness prediction according to Ivanovskii [45]. These models represent semiempirical correlations between the Vickers hardness H_V , and bulk, shear and Young moduli. All models show a general trend where AlCr_2B_2 should be the hardest phase followed by a decrease in hardness as the atomic number of M increases with AlNi_2B_2 as the least hard compound. Irrespective of the model, all thermodynamic stable borides (M=Cr, Mn and Fe) should exhibit hardness values above 17 GPa. For example, using

the relation: $H_V = 0.1475G$, the hardness can be estimated 29.1 GPa (AlCr_2B_2), 24.3 GPa (AlMn_2B_2), 20.5 GPa (AlFe_2B_2), 14.9 GPa (AlCo_2B_2), and 13.6 GPa (AlNi_2B_2).

4.4. *Electronic structure and chemical bonding*

Fig. 5 shows the density of states of the AlM_2B_2 compounds, with M ranging from Cr to Ni, as calculated with the FP-LMTO (RSPt) code. For a few eV below the Fermi level, the valence band has predominantly $3d$ character, while the lower lying states are dominated by B and Al. As the atomic number of the transition metal, Z , increases, the M $3d$ states and consequently the B $2p$ are pushed to lower energy. The width of the $3d$ decreases as well as their occupation increases, which leads to a decrease of the crystal field splitting of the transition metal states with increasing Z .

The calculated magnetic moments of the AlM_2B_2 compounds are shown in Table 6. A good agreement is obtained between the FP-LMTO and PAW results, with the exception of AlCo_2B_2 for which a small but finite moment is found within the former method. The energy difference between a spin-degenerate solution and a spin-polarized solution, with a small net moment is sometimes very small, and this small difference can approach the fine energy differences provided by different electronic structure methods (of order 1 meV/atom) [46]. Unfortunately there are no experimental values with which to compare our calculated magnetic properties for AlCo_2B_2 . The induced moments onto the Al and B sites are negligible. The AlCr_2B_2 and AlNi_2B_2 compounds are found to be nonmagnetic.

In order to discuss the differences in the chemical bonding of different borides, in Fig. 6 we plotted the calculated integral of the crystal orbital Hamilton occupation (COHP), integrated up to the Fermi level (ICOHP) for the AlM_2B_2 and the binary MB compounds (M = Cr, Mn, Fe, Co, Ni), as calculated with the LOBSTER code [22, 23, 24, 25]. In all the borides considered, the B-B bonds have a large values of the COHP function, signaling a high bond-strength, as expected for covalent bonds. The M-M bonds are found to have a much lower values of COHP, which is due to a reduced wavefunction overlap between orbitals centered on these atoms, and a reduced bond-strength. This is consistent with what is known about the chemical bonding of e.g. transition metal carbides [47]. The M-B bond has intermediate values of COHP function, suggesting also an intermediate bond strength.

A clear separation between the B-B bond strengths and the other bonds are observed

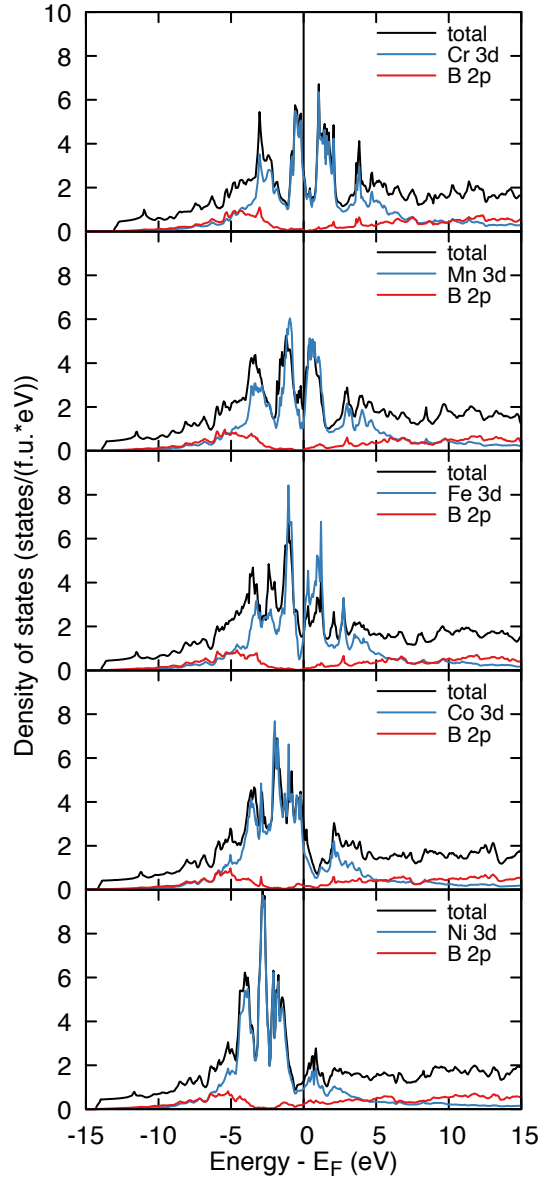


Figure 5: (Color online.) Density of states of the AlM_2B_2 compounds ($M = \text{Cr, Mn, Fe, Co, Ni}$).

not only for the AlM_2B_2 systems, but also for other borides, e.g. the monoborides (Fig. 6b). However, the integrated ICOHP of the binary compounds show much larger variations for the B-B and M-B bonds, compared to the AlM_2B_2 systems, which is possibly due to the fact that the bonds for a three-dimensional network, with varying crystal structures, as is the case of the binary borides, while a quasi-two-dimensional network is formed in the Al-borides. The Mn-B, Fe-B, and Co-B bond strengths in the binary borides stand out, which can be explained by the fact that these compounds crystallize in a different structure compared to CrB and NiB.

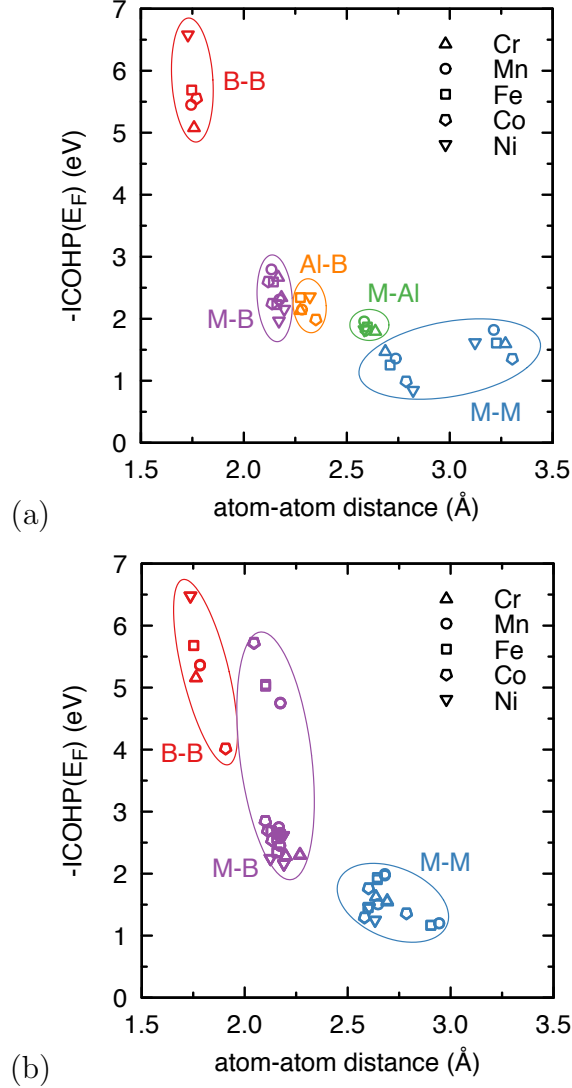


Figure 6: (Color online.) Integrated COHP up to the Fermi level, with reversed sign, for different atom-atom bonds and bond separations in (a) AlM_2B_2 and (b) MB ($M = \text{Cr, Mn, Fe, Co, Ni}$).

The quasi-two-dimensional character of the crystal structure of the Al-borides is evident from Fig. 7a, which shows an isosurface of the AlFe_2B_2 charge density. The largest values of the charge density are within the MB planes, while much lower values are obtained in the Al planes.

The integrated COHP for the AlM_2B_2 series ($M = \text{Cr, Mn, Fe, Co, Ni}$) is shown in Fig. 7b. The B-B bond shows a rather steady increase with increasing Z , while the metal-metal bond strength shows a decrease. The latter may be explained by a filling of the antibonding states as the $3d$ occupation increases along the series, as observed from the COHP calculations. This is in line with Chai et al.'s results [8].

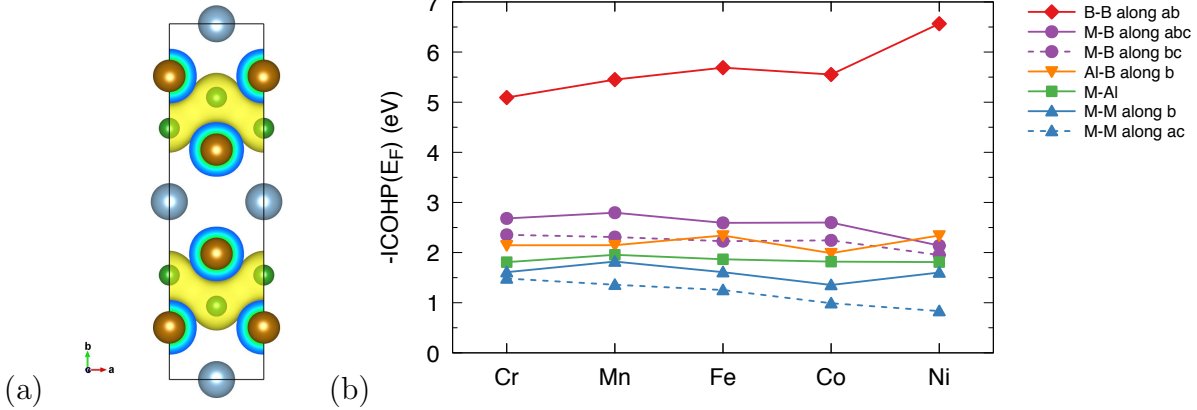


Figure 7: (Color online.) a). Isosurface of the charge density of the AlFe₂B₂. The value of the isosurface was set to 0.09 electrons/Å³. Similar pictures are obtained for the other AlM₂B₂ compounds. b) Integrated COHP up to the Fermi level, with reversed sign, for different bonds in AlM₂B₂.

4.5. Work of separation

In order to gain insight into the background of delamination, we calculated the work of separation (W) in AlM₂B₂ crystals. We separated the crystals (1) between transition metal and aluminium layers, (2) between two boron layers within the M-B slab, and (3) between transition metal and boron layers. As Fig. 8 shows, the work of separation decreases with increasing Z . For all AlM₂B₂ borides, it is energetically most favorable to separate the crystals between the transition metal and aluminium layers, i.e. to break M-Al bonds (four bonds per unit cell), which are weaker than M-B or B-B bonds, as we previously shown in Fig. 7b. The highest work of separation corresponds to breaking the bonds between transition metal and boron layers, except for AlNi₂B₂, where we obtained the highest energy for separating the crystal between two boron layers. This is due to the fact that upon separation between M and B layers, six M-B bonds per unit cell are broken, while separation between two boron layers involves breaking of two B-B bonds per unit cell. AlNi₂B₂ has the strongest B-B bonds of all AlM₂B₂ borides (see Fig. 7b), in fact, here the B-B bonds are more than three times as strong as the M-B bonds, therefore in this crystal separation between two boron planes requires the highest energy. We have performed a Bader charge analysis of these compounds, and find that the Al atoms have donated electrons, and are therefore positively charged. Hence, there is an ionic contribution to the weaker bond of these atoms.

On final thing should be noted with Fig. 8, namely that the trend of the bond strength

shows a decreasing behavior of the M-B and B-B bond, as the series is traversed. This behavior is not reflected in the trend of Fig. 7b, where the B-B ICOHP curve is increasing along the series. It should be noted that the ICOHP is by no means an exact measure of the chemical binding, it is merely an indicator, while the data in Fig. 8 shows total energy differences, and are more reliable.

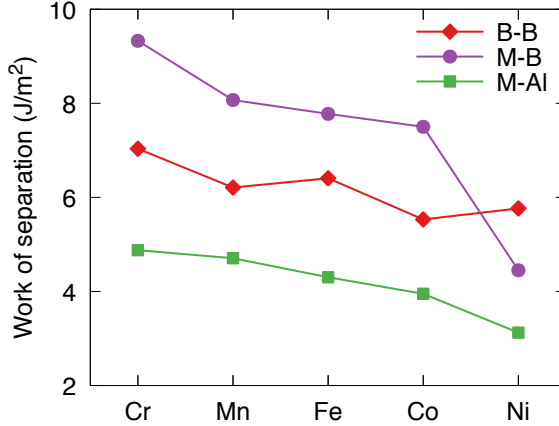


Figure 8: (Color online.) Work of separation in AlM_2B_2 calculated upon separating the crystals between two B planes (diamonds), between M and B planes (circles), and between M and Al planes (squares).

4.6. Experimental results

Samples with a nominal composition AlM_2B_2 (M=Cr, Mn, Fe, Co, Ni) were synthesized by arc-melting followed by annealing (see Section 3). X-ray diffraction (XRD) revealed that AlCr_2B_2 , AlMn_2B_2 , and AlFe_2B_2 were formed. The unit cell parameters are summarized in Table 1 and show a good agreement with calculations, as discussed in Section 4.1. For the experimental synthesis of AlCo_2B_2 , a multiphase sample was observed from the XRD measurements, including an unknown phase. From SEM (not shown), a ternary phase is observed with a similar composition to the expected AlCo_2B_2 (Al 23 at.%, Co 34 at.%, B 43 at.%, measured with SEM-EDS). The unit cell of the unknown phase can be indexed from single crystal diffraction as monoclinic with the cell parameters $a=2.924(4)$ Å, $b=6.107(8)$ Å, $c=8.522(8)$ Å, and $\beta=76.37(9)^\circ$. Unfortunately, due to strong twinning in the sample, we have not been able to solve the complete crystal structure although measurements with single crystal XRD as well as electron diffraction and EDS measurements have been performed. This monoclinic phase decomposes af-

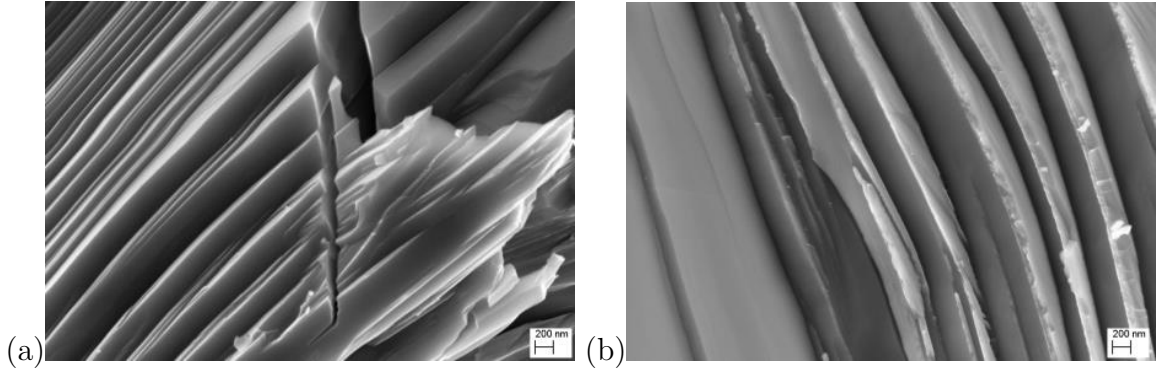


Figure 9: Delamination (a) in AlCr_2B_2 and (b) in AlFe_2B_2 (SEM micrographs).

ter heat treatments (900 °C for 14 d, followed by quenching in cold water), suggesting metastability. For the AlNi_2B_2 sample, no ternary phases similar to AlM_2B_2 were observed. Consequently, our experimental studies confirm the theoretical results in Fig. 2 suggesting only Cr, Mn and Fe form stable AlM_2B_2 borides.

The Vickers hardness of the AlM_2B_2 phases was determined to be 10.4(3) GPa for AlCr_2B_2 , 7.3(3) GPa for AlMn_2B_2 , and 9.5(3) GPa for AlFe_2B_2 . This is in line with recently reported values of 6.0-7.0 GPa for AlCr_2B_2 , 7.0-9.6 GPa for AlMn_2B_2 , and 11.6-14.7 GPa for AlFe_2B_2 [3]. These hardness values are significantly lower than those of transition metal mono- and diborides, which have a Vickers hardness around 20-25 GPa, and also lower than the hardness values estimated from the theoretical results (>17 GPa) using the models in Ref. [45]. As will be discussed below we attribute this deviation is due to a nanolaminated structure similar to the well-known MAX-phases.

We also studied the deformation of AlCr_2B_2 and AlFe_2B_2 in SEM by pressing a sharp tool into the surface of a polished sample. SEM micrographs of the damaged areas show a clear laminated fracture behavior (see Fig. 9). A clear difference in deformation behavior was observed for AlCr_2B_2 and AlFe_2B_2 . AlCr_2B_2 has more cracks and thinner flakes than AlFe_2B_2 . The AlMn_2B_2 sample showed similar delamination phenomena as AlFe_2B_2 , but to a lesser extent due to a less well sintered sample, and is not shown here.

5. Discussion of the nanolaminate behavior of AlM_2B_2

The theoretical results clearly show that AlM_2B_2 ternary borides represent nanolaminated systems. These borides have a layered structure where M-B slabs are separated by

Al layers. The M-B slabs incorporate strong covalent B-B and M-B bonds, which gives a very strong cohesion to these slabs. The interlayer Al-B and M-B bonds, however, are much weaker, compared to the sum of B-B and M-B bonds within the M-B slabs. This makes delamination possible. All AlM_2B_2 compounds have a significantly larger electron density in the M-B slabs than in the Al layers and between Al layers and M-B slabs. Thus, delamination is expected to occur between M-B slabs and Al layers in all ternary borides. This is supported by the calculated work of separation in these borides. We found that all AlM_2B_2 crystals are easiest to separate between the transition metal and aluminium layers. For the stable AlM_2B_2 borides, this requires about 2 J/m² less energy than separation between two boron layers, and about 4 J/m² less energy than separation between the transition metal and boron layers.

Theoretical models estimating hardness from elastic constants [45], which are able to roughly reproduce hardness of e.g. transition metal diborides, predict significantly higher hardness (above 17 GPa) for the stable AlM_2B_2 borides, than the measured Vickers hardness, which is 10.4(3) GPa for AlCr_2B_2 , 7.3(3) GPa for AlMn_2B_2 , and 9.5(3) GPa for AlFe_2B_2 . Furthermore, the measured Vickers hardness of AlM_2B_2 is significantly lower than those of transition metal mono- and diborides. These differences between calculated and measured hardness, as well as between the measured hardness of ternary AlM_2B_2 borides and transition metal mono- and diborides are due to the ability of AlM_2B_2 borides for delamination. This is similar to MAX phases, where the nanolaminated MAX phases have a reduced Vickers hardness of around 5-6 GPa, compared to the 20-30 GPa hardness of transition metal carbides. In contrast to the MAX-phases no kink or shear band deformation can be observed.

Finally, we presented experimental evidence of delamination in AlCr_2B_2 and AlFe_2B_2 (see Fig. 9). We found more cracks in AlCr_2B_2 (Fig. 9a) than in AlFe_2B_2 (Fig. 9b). This is in agreement with the theoretical elastic constants, namely that AlCr_2B_2 has higher c_{11} (552.2 GPa) than AlFe_2B_2 with a c_{11} of 447.0 GPa, i.e. to distort the AlCr_2B_2 crystal along the crystallographic axis a , requires more energy than in AlFe_2B_2 . This in turn can lead to easier crack formation in AlCr_2B_2 . Figure 9 also shows that there are more flakes in the delaminated AlCr_2B_2 sample than in AlFe_2B_2 , suggesting that it should be easier to delaminate AlCr_2B_2 . This is in line with the theoretically predicted

M-Al bond strengths, namely we obtained a lower -ICOHP for the Cr-Al than the Fe-Al bonds, suggesting that the Cr-Al bond is weaker than the Fe-Al bond. However, we calculated slightly higher work of separation for AlCr_2B_2 than for AlFe_2B_2 (Fig. 7b), which seems to be in contradiction with the experimental results. We speculate that in order to predict the energetics of delamination, the additional factor of chemical bonding has to be included. When delamination occurs, the freshly exposed surfaces will rapidly adsorb e.g. oxygen forming metal-oxygen bonds and eventually surface oxides. This is an exothermic reaction and the total delamination process will therefore be influenced by the sum of the energy cost to break M-Al bonds and energy gain upon forming surface oxides. In fact, the enthalpy of formation of e.g. Cr_2O_3 (-1140 kJ/mol) is lower than that of Fe_2O_3 (-824 kJ/mol), therefore the energy gain to form Cr_2O_3 would be larger. Thus, it could be energetically more favorable to delaminate AlCr_2B_2 .

6. Conclusions

In this study we have examined the phase stability and elastic properties of ternary borides, namely AlCr_2B_2 , AlMn_2B_2 , AlFe_2B_2 , AlCo_2B_2 , and AlNi_2B_2 . We calculated their unit cell parameters and found a good agreement between theoretical and measured experimental cell parameters. The phase stability of the borides has also been investigated theoretically, and we find that AlCr_2B_2 , AlMn_2B_2 , and AlFe_2B_2 are stable, while AlCo_2B_2 , and AlNi_2B_2 are metastable phases. We calculated the elastic properties of all compounds, as well, and found that all the borides are mechanically stable, as their elastic constants fulfill the stability criteria. The bulk modulus to shear modulus ratio, B/G , increases from AlCr_2B_2 to AlNi_2B_2 , i.e. the borides become more ductile for the heavier compounds. The first three borides in the series, AlCr_2B_2 , AlMn_2B_2 , and AlFe_2B_2 are more brittle, while AlCo_2B_2 and AlNi_2B_2 are more ductile. We proposed that the mechanical properties of AlFe_2B_2 could be improved, namely shifted towards ductile behavior, by alloying it with cobalt or nickel, or a combination of them. Our results suggest that $\text{Al}(\text{Fe}_x\text{Co}_{1-x})_2\text{B}_2$, $\text{Al}(\text{Fe}_x\text{Ni}_{1-x})_2\text{B}_2$, or even $\text{Al}(\text{Fe}_x\text{Co}_y\text{Ni}_{1-x-y})_2\text{B}_2$ could be stable, and at the same time have improved elasticity compared to pure AlFe_2B_2 .

The chemical bonding in these layered ternary borides was investigated theoretically by several tools, and we found strong covalent B-B and M-B bonds in the M-B layers, and

weaker bonds between M-B and Al layers. Accordingly, all AlM_2B_2 borides have high electron density in the M-B slabs, and significantly lower density in the Al layers and between Al layers and M-B slabs. The chemical bonding of Al in these compounds have a significant ionic component. We also calculated the work of separation between B-B, M-B and M-Al planes, and found that all AlM_2B_2 crystals are easiest to separate between the transition metal and aluminium layers, and we have predicted that delamination occurs between the M-B slabs and the Al layers.

The Vickers hardness we detected for the experimental samples, varies between 7.3 and 10.4 GPa, which is about 30% of the hardness of transition metal mono- and diborides. This significant reduction in hardness is due to their nanolaminated structure. Finally, applying SEM measurements, we demonstrated that AlCr_2B_2 and AlFe_2B_2 indeed show a laminated fracture behavior.

Acknowledgements

The Swedish Research Council is acknowledged for financial support. O.E. also acknowledges financial support from VR, eSENCE and the KAW (projects 2013.0020 and 2012.0031). We also acknowledge the Swedish National Infrastructure for Computing (SNIC) for the allocation of time in high performance supercomputers at NSC, HPC2N and PDC.

Table 1: Theoretical and experimental unit cell parameters (in Å) and volumes (in Å³) of AlM₂B₂ (M=Cr, Mn, Fe, Co, Ni).

Substance	a_{theor}	b_{theor}	c_{theor}	V_{theor}	a_{expt}	b_{expt}	c_{expt}	V_{expt}
AlCr ₂ B ₂	2.9232	11.0511	2.9334	94.7622	2.9387(3)	11.0605(11)	2.9714(3)	96.58(2)
AlMn ₂ B ₂	2.8949	11.0750	2.8306	90.7519	2.9231(2)	11.0698(9)	2.8993(2)	93.82(1)
AlFe ₂ B ₂	2.9162	11.0225	2.8515	91.6581	2.9258(4)	11.0278(9)	2.8658(3)	92.46(2)
AlCo ₂ B ₂	2.9659	11.3303	2.6833	90.1711				
AlNi ₂ B ₂	2.9779	11.0403	2.8497	93.6893				

Table 2: Theoretical single crystal elastic constants (c_{ij} in GPa) of AlM₂B₂ (M=Cr, Mn, Fe, Co, Ni).

Substance	c_{11}	c_{22}	c_{33}	c_{44}	c_{55}	c_{66}	c_{12}	c_{13}	c_{23}
AlCr ₂ B ₂	552.2	495.7	478.6	198.3	221.5	195.8	124.0	133.5	147.3
AlMn ₂ B ₂	486.0	413.1	478.4	152.2	192.2	186.9	193.5	132.1	140.0
AlFe ₂ B ₂	447.0	402.7	334.6	140.2	166.3	156.2	170.1	133.9	156.4
AlCo ₂ B ₂	380.2	317.1	319.9	127.6	153.1	102.2	193.3	199.0	186.9
AlNi ₂ B ₂	375.5	332.7	253.4	110.2	101.4	118.7	154.8	168.6	178.9

Table 3: Theoretical bulk moduli (B in GPa), shear moduli (G in GPa), Young's moduli (E in GPa), Poisson ratios (ν), and B/G ratios of AlM_2B_2 (M=Cr, Mn, Fe, Co, Ni).

Substance	B	G	E	ν	B/G	
AlCr_2B_2	259.6	197.9	473.4	0.20	1.31	Voight
	259.2	196.3	470.2	0.20	1.32	Reuss
	259.4	197.1	471.8	0.20	1.32	Hill
AlMn_2B_2	256.5	167.0	411.8	0.23	1.54	Voight
	255.5	162.6	402.5	0.24	1.57	Reuss
	256.0	164.8	407.1	0.23	1.55	Hill
AlFe_2B_2	233.9	140.8	351.8	0.25	1.66	Voight
	229.6	136.9	342.5	0.25	1.68	Reuss
	231.8	138.8	347.2	0.25	1.67	Hill
AlCo_2B_2	241.7	105.8	277.0	0.31	2.28	Voight
	239.4	96.3	254.7	0.32	2.49	Reuss
	240.5	101.0	265.9	0.32	2.38	Hill
AlNi_2B_2	218.5	96.7	252.8	0.31	2.26	Voight
	213.8	87.8	231.7	0.32	2.43	Reuss
	216.1	92.2	242.3	0.31	2.34	Hill

Table 4: Theoretical Cauchy pressures (P_a , P_b , P_c in GPa) of AlM_2B_2 (M=Cr, Mn, Fe, Co, Ni).

	AlCr_2B_2	AlMn_2B_2	AlFe_2B_2	AlCo_2B_2	AlNi_2B_2
P_a	-50.99	-12.26	16.19	59.24	68.68
P_b	-87.99	-60.05	-32.41	45.86	67.14
P_c	-71.71	6.59	13.92	91.09	36.12

Table 5: Theoretical shear anisotropic factors (A_1 , A_2 , A_3), anisotropy in compressibility (A_B , in %), anisotropy in shear (A_G , in %), and universal elastic anisotropy index (A_u) of AlM_2B_2 (M=Cr, Mn, Fe, Co, Ni).

	$AlCr_2B_2$	$AlMn_2B_2$	$AlFe_2B_2$	$AlCo_2B_2$	$AlNi_2B_2$
A_1	1.04	0.87	1.09	1.69	1.51
A_2	1.30	1.26	1.57	2.33	1.78
A_3	0.98	1.46	1.23	1.32	1.19
A_B	0.08	0.20	0.93	0.49	1.09
A_G	0.40	1.34	1.42	4.72	4.82
A_u	0.04	0.14	0.16	0.50	0.53

Table 6: Calculated magnetic moments for the AlM_2B_2 compounds using FP-LMTO (RSPt) and PAW (VASP).

System	μ/M (RSPt)	$\mu/f.u.$ (RSPt)	μ/M (VASP)	$\mu/f.u.$ (VASP)
$AlMn_2B_2$	0.39	0.75	0.43	0.82
$AlFe_2B_2$	1.35	2.67	1.37	2.70
$AlCo_2B_2$	0.19	0.39	0.15	0.31

References

- [1] M. Barsoum, The $m_{N+1}ax_n$ phases: A new class of solids; thermodynamically stable nanolaminates, *Prog. Solid State Chem.* 28 (2000) 201–281.
- [2] R. Telle, A. Momozawa, D. Music, J. Schneider, Boride-based nano-laminates with max-phase-like behaviour, *J. Solid State Chem.* 179 (2006) 2850–2857.
- [3] M. Ade, H. Hillebrecht, Ternary borides cr_2alb_2 , cr_3alb_4 , and cr_4alb_6 : The first members of the series $(crb_2)ncral$ with $n = 1, 2, 3$ and a unifying concept for ternary borides as mab-phases, *Inorg. Chem.* 54 (2015) 6122–6135.
- [4] S. Kota, E. Zapata-Solvas, A. Ly, J. Lu, O. Elkassabany, A. Huon, W. E. Lee, L. Hultman, S. J. May, M. W. Barsoum, Synthesis and characterization of an alumina forming nanolaminated boride: $Moalb$, *Sci. Rep.* 6 (2016) 26475.
- [5] J. Lu, S. Kota, M. Barsoum, L. Hultman, Atomic structure and lattice defects in nanolaminated ternary transition metal borides, *Mater. Res. Lett.* (2016).
- [6] X. Tan, P. Chai, C. M. Thompson, M. Shatruk, Magnetocaloric effect in $alfe_2b_2$: Toward magnetic refrigerants from earth-abundant elements, *J. Am. Chem. Soc.* 135 (2013) 9553–9557.
- [7] J. Cedervall, M. S. Andersson, T. Sarkar, E. K. Delczeg-Czirjak, L. Bergqvist, T. C. Hansen, P. Beran, P. Nordblad, M. Sahlberg, Magnetic structure of the magnetocaloric compound $alfe_2b_2$, *Journal of Alloys and Compounds* 664 (2016) 784–791.
- [8] P. Chai, S. A. Stoian, X. Tan, P. A. Dube, M. Shatruk, Investigation of magnetic properties and electronic structure of layered-structure borides alt_2b_2 ($t=fe, mn, cr$) and $alfe_2xmnxb_2$, *J. Solid State Chem.* 224 (2015) 52–61.
- [9] L. Nie, W. Zhou, Y. Zhan, Theoretical investigation of the $alcrb$ orthorhombic ternary compounds, *Computational and Theoretical Chemistry* 1020 (2013) 51–56.
- [10] Y. Cheng, Z. Lv, X. Chen, L. Cai, Structural, electronic and elastic properties of $alfe_2b_2$: First-principles study, *Comp. Mat. Sci.* 92 (2014) 253–257.
- [11] P. E. Blöchl, Projector augmented-wave method 50 (1994) 17953–17979.

- [12] G. Kresse, D. Joubert, From ultrasoft pseudopotentials to the projector augmented-wave method, *Phys. Rev. B* 59 (1999) 1758.
- [13] G. Kresse, J. Hafner, Ab initio molecular dynamics for liquid metals 47 (1993) 558–561.
- [14] G. Kresse, J. Furthmüller, Efficiency of ab-initio total energy calculations for metals and semiconductors using a plane-wave basis set, *Comp. Mat. Sci.* 6 (1996) 15–50.
- [15] G. Kresse, J. Furthmüller, Efficient iterative schemes for ab initio total-energy calculations using a plane-wave basis set 54 (1996) 11169–11186.
- [16] P. Hohenberg, W. Kohn, Inhomogeneous electron gas, *Phys. Rev.* 136 (1964) B864–B871.
- [17] W. Kohn, L. Sham, Self-consistent equations including exchange and correlation effects 140 (1965) A1133–A1138.
- [18] J. P. Perdew, K. Burke, M. Ernzerhof, Generalized gradient approximation made simple 77 (1996) 3865–3868.
- [19] P. Ravindran, L. Fast, P. A. Korzhavyi, B. Johansson, J. Wills, O. Eriksson, Density functional theory for calculation of elastic properties of orthorhombic crystals: Application to TiSi_2 , *J. Appl. Phys.* 84 (1998) 4891–4904.
- [20] O. K. Andersen, Linear methods in band theory, *Physical Review B* 12 (1975) 3060–3083.
- [21] J. M. Wills, O. Eriksson, P. Andersson, A. Delin, O. Grechnev, M. Alouani, Full-Potential Electronic Structure Method, volume 167 of *Springer Series in Solid-State Sciences*, Springer Berlin Heidelberg, Berlin, Heidelberg, 2010.
- [22] R. Dronskowski, P. E. Bloechl, Crystal orbital Hamilton populations (COHP): energy-resolved visualization of chemical bonding in solids based on density-functional calculations, *J. Phys. Chem.* 97 (1993) 8617–8624.

- [23] V. L. Deringer, A. L. Tchougréeff, R. Dronskowski, Crystal Orbital Hamilton Population (COHP) Analysis As Projected from Plane-Wave Basis Sets, *J. Phys. Chem. A* 115 (2011) 5461–5466.
- [24] S. Maintz, V. L. Deringer, A. L. Tchougréeff, R. Dronskowski, Analytic projection from plane-wave and PAW wavefunctions and application to chemical-bonding analysis in solids, *J. Comput. Chem.* 34 (2013) 2557–2567.
- [25] S. Maintz, V. L. Deringer, A. L. Tchougréeff, R. Dronskowski, LOBSTER: A tool to extract chemical bonding from plane-wave based DFT, *J. Comput. Chem.* 37 (2016) 1030–1035.
- [26] M. ElMassalami, D. da S. Oliveira, H. Takeya, On the ferromagnetism of AlFe_2B_2 , *J. Magn. Magn. Mat.* 323 (2011) 2133–2136.
- [27] T. J. B. Holland, S. A. T. Redfern, Unit cell refinement from powder diffraction data; the use of regression diagnostics, *Miner. Mag.* 61 (1997) 65–77.
- [28] W. Jeitschko, The crystal structure of Fe_2AlB_2 , *Acta Cryst. B* 25 (1969) 163–165.
- [29] E. J. Felten, The preparation of aluminum diboride, AlB_2 , *J. Am. Chem. Soc.* 78 (1956) 5977–5978.
- [30] R. Kiessling, The borides of manganese, *Acta Chem. Scand.* 4 (1950) 146–159.
- [31] T. Bjurström, Röntgenanalyse der systeme eisen-bor, kobalt-bor und nickel-bor, *Ark. Kemi Mineral. Geol.* 11A (1933) 1–12.
- [32] S. Okada, T. Atoda, I. Higashi, Structural investigation of Cr_2B_3 , Cr_3B_4 , and CrB by single-crystal diffractometry, *J. Solid State Chem.* 68 (1987) 61–67.
- [33] E. Lugscheider, O. Knotek, H. Reimann, The ternary system nickel—chromium—boron, *Monatshefte für Chemie / Chemical Monthly* 105 (1974) 80–90.
- [34] A. Kallel, Ordre antiferromagnétique dans les alliages $\text{Cr}_2\text{-xfexal}$, *C.R. Seances Acad. Sci., Ser. B* 268 (1969) 455–458.
- [35] A. Kontio, P. Coppens, New study of the structure of MnAl_6 , *Acta Cryst. B* 37 (1981) 433–435.

- [36] A. V. der Kraan, K. Buschow, The ^{57}Fe Mossbauer isomer shift in intermetallic compounds of iron, *Physica B+C* 138 (1986) 55–62.
- [37] H. Ipsier, A. Mikula, On the ternary b_2 -phase in the Al-Co-Ga system, *Monatshefte für Chemie / Chemical Monthly* 123 (1992) 509–513.
- [38] Y. Dutchak, V. Chekh, High temperature x-ray diffraction study of the lattice dynamics of the compounds AlCo and AlNi, *Russ. J. Phys. Chem.* 55 (1981) 1326–1328.
- [39] F. Mouhat, F.-X. Coudert, Necessary and sufficient elastic stability conditions in various crystal systems, *Phys. Rev. B* 90 (2014) 224104.
- [40] W. Voigt, *Lehrbuch der Kristallphysik*, Teubner, Leipzig, 1928.
- [41] A. Reuss, Account of the liquid limit of mixed crystals on the basis of the plasticity condition for single crystal, *Z. Angew. Math. Mech.* 9 (1929) 49–58.
- [42] V. Tvergaard, J. Hutchinson, Microcracking in ceramics induced by thermal expansion or elastic anisotropy, *J. Am. Ceram. Soc.* 71 (1988) 157–166.
- [43] D. H. Chung, W. R. Buessem, in: F. W. Vahldiek, S. A. Mersol (Eds.), *Anisotropy in Single Crystal Refractory Compound*, volume 2, Plenum, New York, 1968, p. 217.
- [44] S. I. Ranganathan, M. Ostoja-Starzewski, Universal elastic anisotropy index, *Phys. Rev. Lett.* 101 (2008) 055504.
- [45] A. Ivanovskii, Hardness of hexagonal AlB_2 -like diborides of s, p and d metals from semi-empirical estimations, *International Journal of Refractory Metals and Hard Materials* 36 (2013) 179–182.
- [46] K. Lejaeghere, G. Bihlmayer, T. Björkman, P. Blaha, S. Blügel, et al., Reproducibility in density functional theory calculations of solids, *Science* 351 (2016).
- [47] D. L. Price, B. R. Cooper, Total energies and bonding for crystallographic structures in titanium-carbon and tungsten-carbon systems, *Phys. Rev. B* 39 (1989) 4945–4957.